A SIMULATION MODEL FOR THE ANALYSIS OF TRANSIENT MAGNETIC BEARING PERFORMANCE

Myounggyu D. Noh
Dept. Mechatronics Engineering, Chungnam National University, Taejon, Korea, mnoh@cnu.ac.kr

Dominick T. Montie and Eric H. Maslen
Dept. Mechanical, Aerospace and Nuclear Engineering, University of Virginia, Charlottesville, Virginia, USA

Anthony Kondoleon
Draper Laboratories, Cambridge, MA, USA

ABSTRACT

A simulation model for radial magnetic bearings is presented. The model incorporates hysteresis, saturation and eddy current effects. A simple magnetization model is proposed to describe hysteresis and saturation. Eddy currents are assumed to be generated by single–turn fictitious coils wrapped around magnetic flux paths. The dynamic equations describing the simulation model can easily incorporate the operation of switching power amplifier. A simulation of a typical 8–pole radial magnetic bearing produces magnetization curve and switching waveforms very similiar to the experimental observation.

INTRODUCTION

When a magnetic bearing design is evaluated, an idealized linear magnetic model is usually used while neglecting such effects as saturation, hysteresis and eddy currents. However, this idealized model becomes less accurate if the bearing is required to operate in conditions where the effects of hysteresis, saturation and eddy currents become significant. For example, when a self–sensing magnetic bearing is implemented by utilizing the switching waveforms, the performance of the bearing as a sensor can be greatly affected by saturation, hysteresis and eddy currents in terms of sensitivity and repeatability [6, 7]

In this paper, we present a simulation model which includes the effects of saturation, hysteresis and eddy currents. Following the work of Springer, et. al. [3], we adopt a somewhat more convenient hysteresis model and add a simple eddy current model. The eddy current model turns out to be important in that it resolves a number of rank deficiencies which arise in the magnetics model. In addition, we explicitly embed a switching amplifier model which produces switching waveforms. The model produces the switching waveforms very similar to those obtained experimentally, which is essential in evaluating the performance of self-sensing algorithms based on the switching waveform.

MAGNETIC PROPERTIES OF MATERIAL

Hysteresis and Saturation Model

The literature contains numerous models of the magnetic hysteresis phenomenon, notably those of Hodgdon[1], and of Jiles and Atherton[2]. Although these models are capable of describing complicated magnetization processes, they are usually given as differential equations or integral equations. Therefore, the nonlinearity only becomes obvious after solving the equations either analytically or numerically. This complexity makes it difficult to employ these models for the purpose of assessing the effects of magnetic nonlinearity on the performance of the bearing. In this paper, a different nonlinear magnetization model is used. The model is presented by a set of analytic functions. Once the parameters describing the model are identified through curve–fitting the experimental data, the model properly predicts the magnetization process without needing to solve additional equations.

The model assumes that the $B-H$ curve is confined by two envelopes represented by

$$H_1(B) = \frac{B}{\mu_o \mu_r^0} + \frac{\sigma}{\mu_o}\left(1 - \frac{1}{\mu_r^0}\right)\log(1 + \eta \cdot e^{(B-B_s)/\sigma}) + H_r \tag{1}$$

$$H_2(B) = \frac{B}{\mu_o \mu_r^0} - \frac{\sigma}{\mu_o}\left(1 - \frac{1}{\mu_r^0}\right)\log(1 + \eta \cdot e^{(-B-B_s)/\sigma}) - H_r \tag{2}$$

An inspection of (1) and (2) reveals that they are composed of two asymptotes. One of these asymptotes represents the linear portion where flux density is less than

saturation and has a slope of $\mu_0\mu_r$: quite high for very permeable materials like HiMu80. The other asymptote represents the saturation region in which the slope of the $B-H$ curve converges to the permeability of free space, μ_0. The parameter σ controls the sharpness of the transition from one region to the other. The value of η can be determined from the intercept of the asymptote for large flux density on B axis. The separation between these two curves, represented by H_r controls the maximum depth (in the $H-$ direction) of the hysteresis loops.

The actual magnetization H as a function of flux density B is given by

$$H(B) = \begin{cases} H_1(B) - [H_1(B_0) - H(B_0)] \cdot e^{-\beta|B-B_o|} & \text{if } \dot{B} \geq 0 \\ H_2(B) - [H_2(B_0) - H(B_0)] \cdot e^{-\beta|B-B_o|} & \text{if } \dot{B} < 0 \end{cases} \quad (3)$$

where B_o is the flux density at the instant that $\dot{B}$ changes its sign. The parameter β determines the shape of the actual $B-H$ curve. A "soft" magnetic material can be represented by (3) with smaller β, whereas a "hard" magnetic material will be described with larger β. Given the actual $B-H$ for the core material, one can easily identify these parameters.

One can determine the parameters of the hysteresis model by fitting the simulated magnetization curve with the experimental data. Various optimization techniques can be used for this purpose. In this paper, a simplex method is employed. Using the experimental $B-H$ curve for HiMu80, the following parameters were determined from the simplex search:

μ_r	94300	
η	0.0109	
σ	0.0598	Tesla
B_s	0.797	Tesla
β	15.02	Tesla^{-1}
H_r	4.456	Ampére-turns/meter

Figure 1 shows the magnetization model for HiMu80 (solid line) compared with experimental data (crosses).

Eddy Current Model

The effect of eddy currents can be modeled in several ways. One approach would be to use rate–dependent permeability for the stator material [4]. In this paper, it is assumed that eddy currents are generated from single–turn fictitious coils wrapped around the flux paths [5]. The accuracy of this eddy current model depends on the correct estimation of the amount of flux linked by this eddy current loop and its electrical resistance determines the eddy current effects. Recognizing that each eddy current loop stays within a given lamination of the core, the total flux linked by the fictitious coils would reduce by the ratio between the thickness of the lamination and the thickness of

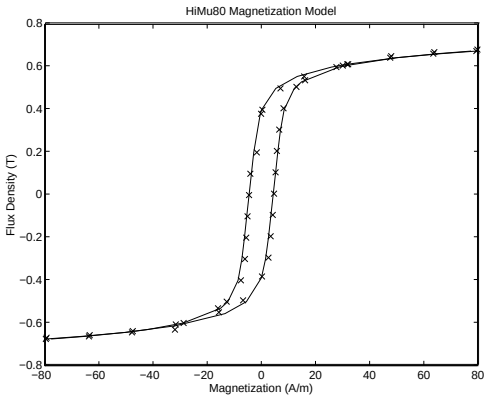

FIGURE 1: Magnetization model for HiMu80.

the lamination stack. However, this ratio overestimates the driving flux because the eddy currents are not perfectly concentrated on the surface. Assuming the eddy currents are uniformly distributed throughout a characteristic *skin depth* δ, the flux linked would be

$$\phi_{ec} = \left(\frac{t_{lam} - \delta}{t_{stack}}\right)\phi \quad (4)$$

The resistance seen by the eddy currents is roughly the stator resistivity, ρ, times the mean current path length divided by the area. For a pole of length l parallel to the flux and width w perpendicular to the flux and to the lamination direction, the resistance would be approximated by

$$r_{ec} = \frac{2\rho w}{l\delta} \quad (5)$$

SIMULATION MODEL

Governing equations

In this paper, a model for an 8–pole radial magnetic bearing is developed. This model can be easily modified to describe radial magnetic bearings with any number of poles. Figure 2 shows all the flux paths of an 8–pole radial magnetic bearing. Applying Faraday's law to the two adjacent coils wired in series, we have

$$n\frac{d\phi_{2i-1}}{dt} - n\frac{d\phi_{2i}}{dt} = V_i - 2ri_i, \quad i = 1,\ldots,4 \quad (6)$$

where n is the number of coil turns in each pole and r is the resistance of the each coil. This equation assumes that all eight coils have identical numbers of turns and coil resistances.

As noted above, the eddy currents are assumed to be generated by a fictitious coils wrapped around the flux paths. Faraday's law for these fictitious coils gives

$$\alpha\frac{d\phi_i}{dt} = -r_{ec_i}i_{ec_i}, \quad i = 1,\ldots,24 \quad (7)$$

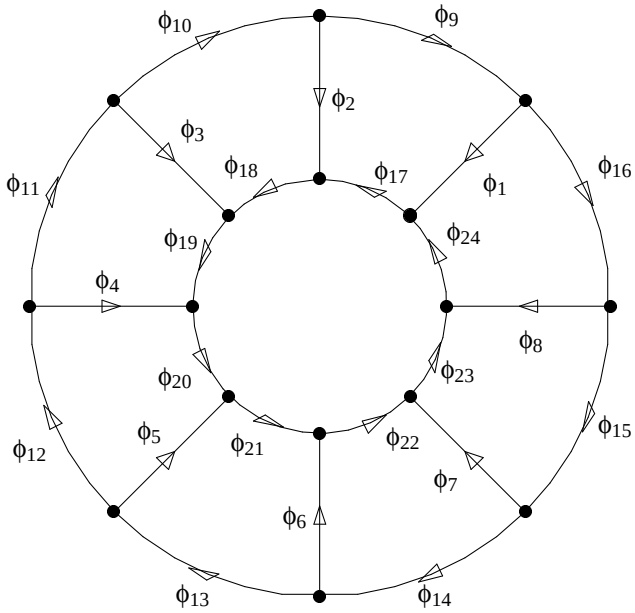

FIGURE 2: Numbering of each magnetic path in 8-pole bearing.

where α is defined in (4) as

$$\alpha = \frac{t_{lam} - \delta}{t_{stack}}$$

The above two equations (6) and (7) can be grouped into one matrix equation.

$$\begin{bmatrix} W^T N \\ \alpha I \end{bmatrix} \frac{d\phi}{dt} = Bv - \begin{bmatrix} W^T R W & 0_{4\times 24} \\ 0_{24\times 4} & R_{ec} \end{bmatrix} i \qquad (8)$$

in which W is the interconnection matrix and R_{ec} is the eddy current resistance matrix.

The vector ϕ in (8) has 24 elements, which can be reduced to 9 using conservation of flux. Following the numbering scheme illustrated in Figure 2, conservation of flux produces 15 equations:

$$\begin{gathered} \phi_k + \phi_{k+7} - \phi_{k+8} = 0, \quad k = 2,\ldots,8 \\ \phi_k + \phi_{k+15} - \phi_{k+16} = 0, \quad k = 2,\ldots,8 \\ \phi_1 + \phi_2 + \cdots + \phi_8 = 0 \end{gathered}$$

In matrix form, the above fifteen equations can be written as

$$C\phi = 0 \qquad (9)$$

Then, using the orthogonal complement of C,

$$\phi = C_\perp^T \hat{\phi} \qquad (10)$$

Whether the magnetic material is linear or not, the constitutive law can be written as

$$H = \mathcal{H}(\phi) \qquad (11)$$

For the air gaps,

$$H_g = \frac{1}{\mu_o A}\phi$$

For the stator paths,

$$H = \frac{1}{\mu_o \mu_r(\phi) A}\phi$$

Ampère's loop law provides additional 9 equations.

$$\begin{gathered} l_k H_k + g_k H_{g_k} + l_{k+8} H_{k+8} - l_{k+1} H_{k+1} - g_{k+1} H_{g_{k+1}} + \\ l_{k+16} H_{k+16} = n i_k + i_{ec_k} + i_{ec_{k+8}} - n i_{k+1} - i_{ec_{k+1}} + i_{ec_{k+16}}, \\ k = 1,\ldots,7 \end{gathered}$$

$$\begin{gathered} l_9 H_9 + \cdots + l_{16} H_{16} = i_{ec_9} + \cdots + i_{ec_{16}} \\ l_{17} H_{17} + \cdots + l_{24} H_{24} = i_{ec_{17}} + \cdots + i_{ec_{24}} \end{gathered}$$

Similar to conservation of flux, the above nine equations can be written in matrix form,

$$LH + GH_g = Si \qquad (12)$$

The details of the matrices used in the simulation model can be found in the appendix

Dynamic Model

Let K be the pseudo–inverse of the the matrix preceding $d\phi/dt$ in (8).

$$K = \left(\begin{bmatrix} W^T N \\ \alpha I \end{bmatrix} C_\perp^T \right)^\dagger$$

Also, define

$$\mathcal{W} = \begin{bmatrix} W^T R W & 0 \\ 0 & R_{ec} \end{bmatrix}$$

Using the orthogonal complement of K, construct

$$\begin{bmatrix} K_\perp \\ K \end{bmatrix}$$

and pre–multiply it to (8). This produces

$$\begin{bmatrix} 0 \\ \dot{\hat{\phi}} \end{bmatrix} = \begin{bmatrix} K_\perp B \\ KB \end{bmatrix} v - \begin{bmatrix} K_\perp \mathcal{W} \\ K\mathcal{W} \end{bmatrix} i \qquad (13)$$

Decompose current vector into two orthogonal components:

$$i = S^T i_a + S_\perp^T i_\perp$$

Then,

$$\begin{aligned} LH + GH_g &= S[S^T i_a + S_\perp^T i_\perp] \\ &= SS^T i_a \end{aligned}$$

Thus,

$$i_a = (SS^T)^{-1}(LH + GH_g)$$

Substituting the decomposed i into (13), produces

$$\begin{bmatrix} 0 \\ \dot{\hat{\phi}} \end{bmatrix} = \begin{bmatrix} K_\perp B \\ KB \end{bmatrix} v - \begin{bmatrix} K_\perp \mathcal{W} S^T (SS^T)^{-1} L & K_\perp \mathcal{W} S_\perp^T \\ K \mathcal{W} S^T (SS^T)^{-1} L & K \mathcal{W} S_\perp^T \end{bmatrix} \cdot \begin{bmatrix} LH + GH_g \\ i_\perp \end{bmatrix} \quad (14)$$

From the first line of (14),

$$i_\perp = (K_\perp \mathcal{W} S_\perp^T)^{-1} K_\perp B v - (K_\perp \mathcal{W} S_\perp^T)^{-1} K_\perp \mathcal{W} S^T (SS^T)^{-1} (LH + GH_g)$$

Substituting $i_\perp$ into the second line of (14) gives the following two equations:

$$\dot{\hat{\phi}} = P(LH + GH_g) + Qv \quad (15)$$

$$i = D(LH + GH_g) + Ev \quad (16)$$

where

$$P = K\mathcal{W}[S_\perp^T (K_\perp \mathcal{W} S_\perp^T)^{-1} K_\perp \mathcal{W} - I] S^T (SS^T)^{-1}$$
$$Q = K[I - \mathcal{W} S_\perp^T (K_\perp \mathcal{W} S_\perp^T)^{-1} K_\perp] B$$
$$D = [I - S_\perp^T (K_\perp \mathcal{W} S_\perp^T)^{-1} K_\perp \mathcal{W}] S^T (SS^T)^{-1}$$
$$E = S_\perp^T (K_\perp \mathcal{W} S_\perp^T)^{-1} K_\perp B$$

SIMULATION EXAMPLE

An eight pole magnetic radial actuator made of HiMu80 is selected to test the simulation model developed in the previous sections. The eight poles are each of equal proportions and are spaced evenly around the circular journal. The stator laminations have an outer diameter of 119.1 mm (4.610 in.), a backiron radial thickness of 7.62 mm (0.3 in.), a pole width of 7.62 mm (0.3 in.), and a pole length of 30.48 mm (1.2 in.). The lamination thickness is 0.178 mm (0.007 in.), with a total of 57 laminations to provide an axial stator thickness of 10.16 mm (0.4 in.). The diameter of the modeled shaft is 25.4 mm (1.0 in.), and, consistent with backiron and leg width, the journal radial thickness is 7.62 mm (0.3 in.). The nominal radial air gap is 0.127 mm (0.005 in.). Each leg carries a coil with 70 turns of wire.

Given the selected geometry and magnetic materials, three important operating parameters needed to be selected prior to the simulation evaluations. These were the nominal bias current, the power supply voltage, and the effective eddy current skin depth. The first two were chosen in a very straightforward manner. First, it was noted that the iron begins to saturate at a current of about 0.65 amps. On the basis of this observation, the bias current was set at 0.2 amps, consistent with common operating principals. Second, the amplifier voltage was adjusted until the amplitude of the switching waveform was about 10% of the bias current.

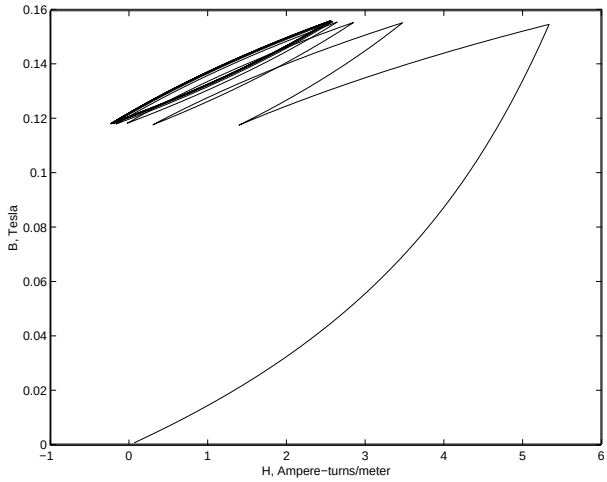

FIGURE 3: Field intensity (H) *vs* flux density (B).

The skin depth was initially selected, rather arbitrarily, to be one quarter of the lamination thickness, 0.04 mm (0.0018 inches). Clearly, the skin depth cannot exceed one half of the lamination thickness and it is expected to diminish in thickness with increased switching frequency. After examination of the resulting switching waveform, it was decided that the depth of the current discontinuity at the switch point was excessive with so large a skin depth. Through an trial and error, the skin depth of 0.013 mm (0.0005 inches) was selected as producing an amount of switch discontinuity consistent with experimental experience. This selection process for the skin depth indicates that the eddy currents are more dominant magnetic nonideality than hysteresis. A parametric study (not shown in this paper) of self–sensing performance with respect to the changes in the skin depth and the magnetic coercivity supports this claim.

With the bearing geometry and parameters described above, a simulation is performed when the coil currents increase from zero to the bias point. Figure 3 shows the transient behaviour of flux density versus field intensity. The simulation results clearly indicate that the $B-H$ curve converges to a *stable* minor hysteresis loop. This means that the switching amplifier causes the field to converge to a stable and repeatible loop on the $B-H$ curve so that the mean $B-H$ relationship would be expected to show no hysteresis. Thus, hysteresis would not affect DC force estimates obtained from the current with no hysteresis model. Note that this apparent stability may be an artifact of the model, but it should be emphasized that no particular effort was taken in developing the model to produce this result. The simulation results of course need

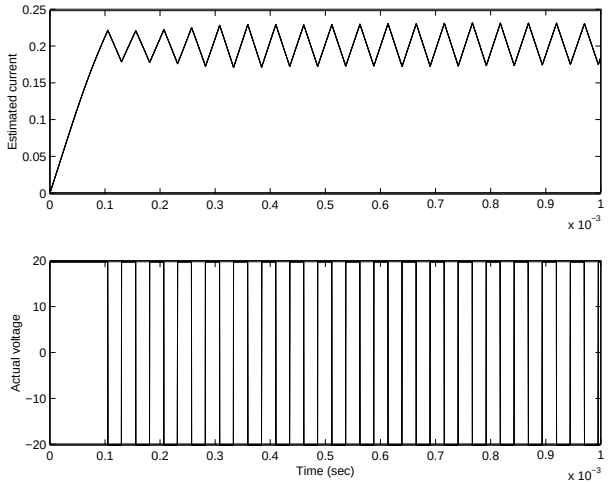

FIGURE 4: Current (I) *vs* time.

to be verified by experiments.

Figure 4 shows the time transients of current and voltage signals produced by the simulation model. The discontinuity due to eddy current effects is better observed if the current waveform is zoomed up as in Figure 5.

CONCLUSION

In this paper, we presented a simulation model for radial magnetic bearings which included the effects of saturation, hysteresis, and eddy currents. The simulation model was derived without making assumptions on power amplifiers. Thus, a switching amplifier could easily handled. The simulation results showed that the model correctly predicted the minor hysteresis loop to which the magnetization curve converges and the discontinuity in the current switching waveforms due to eddy current effects.

Using this simulation model, it would be possible to see the effects of hysteresis and eddy currents on the performance of magnetic bearings operating in severe conditions. Also, a parametric study can be carried out to assess the accuracy of self–sensing magnetic bearings due to eddy currents and hysteresis in various working conditions.

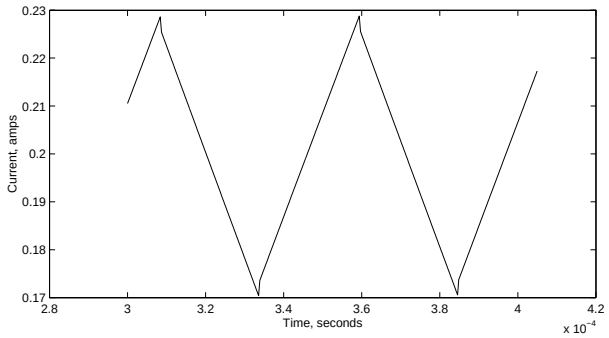

FIGURE 5: Current (I) *vs* time. Illustrates discontinuity induced by eddy current effects.

REFERENCES

[1] M. L. Hodgdon, "Applications of a theory of ferromagnetic hysteresis," *IEEE Transactions on Magnetics*, vol. 24, pp. 218–221, January 1988.

[2] D. C. Jiles and D. L. Atherton, "Theory of ferromagnetic hysteresis," *Journal of Magnetism and Magnetic Materials*, vol. 61, pp. 48–60, 1986.

[3] H. Springer, G. Schlager, and T. Platter, "A Nonlinear Simulation Model for Active Magnetic Bearing Actuators," *in Proceedings of the Sixth International Symposium on Magnetic Bearings*, Cambridge, MA, USA, 1998, pp. 189–203.

[4] D. C. Meeker, E. H. Maslen, and M. D. Noh, "An Augmented Circuit Model for Magnetic Bearings Including Eddy Currents, Fringing, and Leakage," IEEE *Transactions on Magnetics*, Vol. 32, No. 4, July 1996, pp. 3219-3227.

[5] M. D. Noh, *Self–Sensing Magnetic Bearings Driven by a Switching Power Amplifier*. Ph. D. Thesis, The University of Virgnia, 1996.

[6] M. D. Noh and E. H. Maslen, "Self Sensing Active Magnetic Bearings Based on Parameter Estimation," IEEE *Transactions on Instrumentation and Measurement*, 46(1):45-50, February 1997.

[7] Y. Okada, K. Matsuda, and B. Nagai, "Sensorless magnetic levitation control by measuring the PWM carrier frequency component," in *Proceedings of the Third International Symposium on Magnetic Bearings*, 1992.

APPENDIX

Interconnection matrix

$$W_{8\times 4} = \begin{bmatrix} 1 & 0 & 0 & 0 \\ -1 & 0 & 0 & 0 \\ 0 & 1 & 0 & 0 \\ 0 & -1 & 0 & 0 \\ 0 & 0 & 1 & 0 \\ 0 & 0 & -1 & 0 \\ 0 & 0 & 0 & 1 \\ 0 & 0 & 0 & -1 \end{bmatrix} \qquad (17)$$

Coil turn matrix

$$N_{8\times 24} = \begin{bmatrix} n & 0 & \dots & 0 & 0 & \dots & 0 \\ 0 & n & \dots & 0 & 0 & \dots & 0 \\ \vdots & \vdots & \ddots & \vdots & \vdots & & \vdots \\ 0 & 0 & \dots & n & 0 & \dots & 0 \end{bmatrix} \tag{18}$$

Input matrix

$$B_{32\times 4} = \begin{bmatrix} 1 & 0 & 0 & 0 & \dots & 0 \\ 0 & 1 & 0 & 0 & \dots & 0 \\ 0 & 0 & 1 & 0 & \dots & 0 \\ 0 & 0 & 0 & 1 & \dots & 0 \end{bmatrix} \tag{19}$$

Flux conservation matrix

$$C_{15\times 24} = \begin{bmatrix} 0&1&0&0&0&0&0&0&1&-1&0&0&0&0&0&0&0&0&0&0&0&0&0&0 \\ 0&0&1&0&0&0&0&0&0&1&-1&0&0&0&0&0&0&0&0&0&0&0&0&0 \\ 0&0&0&1&0&0&0&0&0&0&1&-1&0&0&0&0&0&0&0&0&0&0&0&0 \\ 0&0&0&0&1&0&0&0&0&0&0&1&-1&0&0&0&0&0&0&0&0&0&0&0 \\ 0&0&0&0&0&1&0&0&0&0&0&0&1&-1&0&0&0&0&0&0&0&0&0&0 \\ 0&0&0&0&0&0&1&0&0&0&0&0&0&1&-1&0&0&0&0&0&0&0&0&0 \\ 0&0&0&0&0&0&0&1&0&0&0&0&0&0&1&-1&0&0&0&0&0&0&0&0 \\ 0&1&0&0&0&0&0&0&0&0&0&0&0&0&0&1&-1&0&0&0&0&0&0&0 \\ 0&0&1&0&0&0&0&0&0&0&0&0&0&0&0&0&1&-1&0&0&0&0&0&0 \\ 0&0&0&1&0&0&0&0&0&0&0&0&0&0&0&0&0&1&-1&0&0&0&0&0 \\ 0&0&0&0&1&0&0&0&0&0&0&0&0&0&0&0&0&0&1&-1&0&0&0&0 \\ 0&0&0&0&0&1&0&0&0&0&0&0&0&0&0&0&0&0&0&1&-1&0&0&0 \\ 0&0&0&0&0&0&1&0&0&0&0&0&0&0&0&0&0&0&0&0&1&-1&0&0 \\ 0&0&0&0&0&0&0&1&0&0&0&0&0&0&0&0&0&0&0&0&0&1&-1&0 \\ 0&0&0&0&0&0&0&0&1&0&0&0&0&0&0&0&0&0&0&0&0&0&1&-1 \\ 1&1&1&1&1&1&1&1&0&0&0&0&0&0&0&0&0&0&0&0&0&0&0&0 \end{bmatrix} \tag{20}$$

Stator length matrix

$$L_{9\times 24} = \begin{bmatrix} l_1 & -l_2 & 0 & 0 & 0 & 0 & 0 & 0 & l_9 & 0 & 0 & 0 & 0 & 0 & 0 & 0 & l_{17} & 0 & 0 & 0 & 0 & 0 & 0 & 0 \\ 0 & l_2 & -l_3 & 0 & 0 & 0 & 0 & 0 & 0 & l_{10} & 0 & 0 & 0 & 0 & 0 & 0 & 0 & l_{18} & 0 & 0 & 0 & 0 & 0 & 0 \\ 0 & 0 & l_3 & -l_4 & 0 & 0 & 0 & 0 & 0 & 0 & l_{11} & 0 & 0 & 0 & 0 & 0 & 0 & 0 & l_{19} & 0 & 0 & 0 & 0 & 0 \\ 0 & 0 & 0 & l_4 & -l_5 & 0 & 0 & 0 & 0 & 0 & 0 & l_{12} & 0 & 0 & 0 & 0 & 0 & 0 & 0 & l_{20} & 0 & 0 & 0 & 0 \\ 0 & 0 & 0 & 0 & l_5 & -l_6 & 0 & 0 & 0 & 0 & 0 & 0 & l_{13} & 0 & 0 & 0 & 0 & 0 & 0 & 0 & l_{21} & 0 & 0 & 0 \\ 0 & 0 & 0 & 0 & 0 & l_6 & -l_7 & 0 & 0 & 0 & 0 & 0 & 0 & l_{14} & 0 & 0 & 0 & 0 & 0 & 0 & 0 & l_{22} & 0 & 0 \\ 0 & 0 & 0 & 0 & 0 & 0 & l_7 & -l_8 & 0 & 0 & 0 & 0 & 0 & 0 & l_{15} & 0 & 0 & 0 & 0 & 0 & 0 & 0 & l_{23} & 0 \\ 0 & 0 & 0 & 0 & 0 & 0 & 0 & 0 & l_9 & l_{10} & l_{11} & l_{12} & l_{13} & l_{14} & l_{15} & l_{16} & 0 & 0 & 0 & 0 & 0 & 0 & 0 & 0 \\ 0 & 0 & 0 & 0 & 0 & 0 & 0 & 0 & 0 & 0 & 0 & 0 & 0 & 0 & 0 & 0 & l_{17} & l_{18} & l_{19} & l_{20} & l_{21} & l_{22} & l_{23} & l_{24} \end{bmatrix} \tag{21}$$

Gap matrix

$$G_{9\times 8} = \begin{bmatrix} g_1 & -g_2 & 0 & 0 & 0 & 0 & 0 & 0 \\ 0 & g_2 & -g_3 & 0 & 0 & 0 & 0 & 0 \\ 0 & 0 & g_3 & -g_4 & 0 & 0 & 0 & 0 \\ 0 & 0 & 0 & g_4 & -g_5 & 0 & 0 & 0 \\ 0 & 0 & 0 & 0 & g_5 & -g_6 & 0 & 0 \\ 0 & 0 & 0 & 0 & 0 & g_6 & -g_7 & 0 \\ 0 & 0 & 0 & 0 & 0 & 0 & g_7 & -g_8 \\ 0 & 0 & 0 & 0 & 0 & 0 & 0 & 0 \\ 0 & 0 & 0 & 0 & 0 & 0 & 0 & 0 \end{bmatrix} \tag{22}$$

Amperè's loop input matrix

$$S_{9\times 28} = \begin{bmatrix} 2n & 0 & 0 & 0 & 1 & -1 & 0 & 0 & 0 & 0 & 0 & 0 & 1&0&0&0&0&0&0&0&1&0&0&0&0&0&0&0 \\ -n & -n & 0 & 0 & 0 & 1 & -1 & 0 & 0 & 0 & 0 & 0 & 0&1&0&0&0&0&0&0&0&1&0&0&0&0&0&0 \\ 0 & 2n & 0 & 0 & 0 & 0 & 1 & -1 & 0 & 0 & 0 & 0 & 0&0&1&0&0&0&0&0&0&0&1&0&0&0&0&0 \\ 0 & n & -n & 0 & 0 & 0 & 0 & 1 & -1 & 0 & 0 & 0 & 0&0&0&1&0&0&0&0&0&0&0&1&0&0&0&0 \\ 0 & 0 & 2n & 0 & 0 & 0 & 0 & 0 & 1 & -1 & 0 & 0 & 0&0&0&0&1&0&0&0&0&0&0&0&1&0&0&0 \\ 0 & 0 & n & -n & 0 & 0 & 0 & 0 & 0 & 1 & -1 & 0 & 0&0&0&0&0&1&0&0&0&0&0&0&0&1&0&0 \\ 0 & 0 & 0 & 2n & 0 & 0 & 0 & 0 & 0 & 0 & 1 & -1 & 0&0&0&0&0&0&1&0&0&0&0&0&0&0&1&0 \\ 0 & 0 & 0 & 0 & 0 & 0 & 0 & 0 & 0 & 0 & 0 & 0 & 1&1&1&1&1&1&1&1&0&0&0&0&0&0&0&0 \\ 0 & 0 & 0 & 0 & 0 & 0 & 0 & 0 & 0 & 0 & 0 & 0 & 0&0&0&0&0&0&0&0&1&1&1&1&1&1&1&1 \end{bmatrix} \tag{23}$$